Accepted manuscript. https://doi.org/10.1016/j.biortech.2023.129818

Assessment of the marine microalga *Chrysochromulina rotalis* as bioactive feedstock cultured in an easy-to-deploy light-emitting-diode-based tubular photobioreactor

Macías-de la Rosa, A.[1], López-Rosales, L.[1,2], Cerón-García, M.C.[1,2], Molina-Miras, A.[1,2], Soriano-Jerez, Y.[1], Sánchez-Mirón, A.[1,2], Seoane, S.[3,4], García-Camacho, F.[1,2*]

[1]Department of Chemical Engineering, [2]Research Centre CIAIMBITAL, University of Almería, 04120 Almería, Spain

[3]Department of Plant Biology and Ecology, 48940 Leioa, Spain, [4]Technology and Research Centre for Experimental Marine Biology and Biotechnology, University of the Basque Country (UPV/EHU),48620 Plentzia, Spain

*Corresponding author: Francisco García Camacho

Address: Department of Chemical Engineering, University of Almería. Carretera Sacramento s/n. E04120, Almería, Spain.

Telephone number: +34 950015303; e-mail address: fgarcia@ual.es

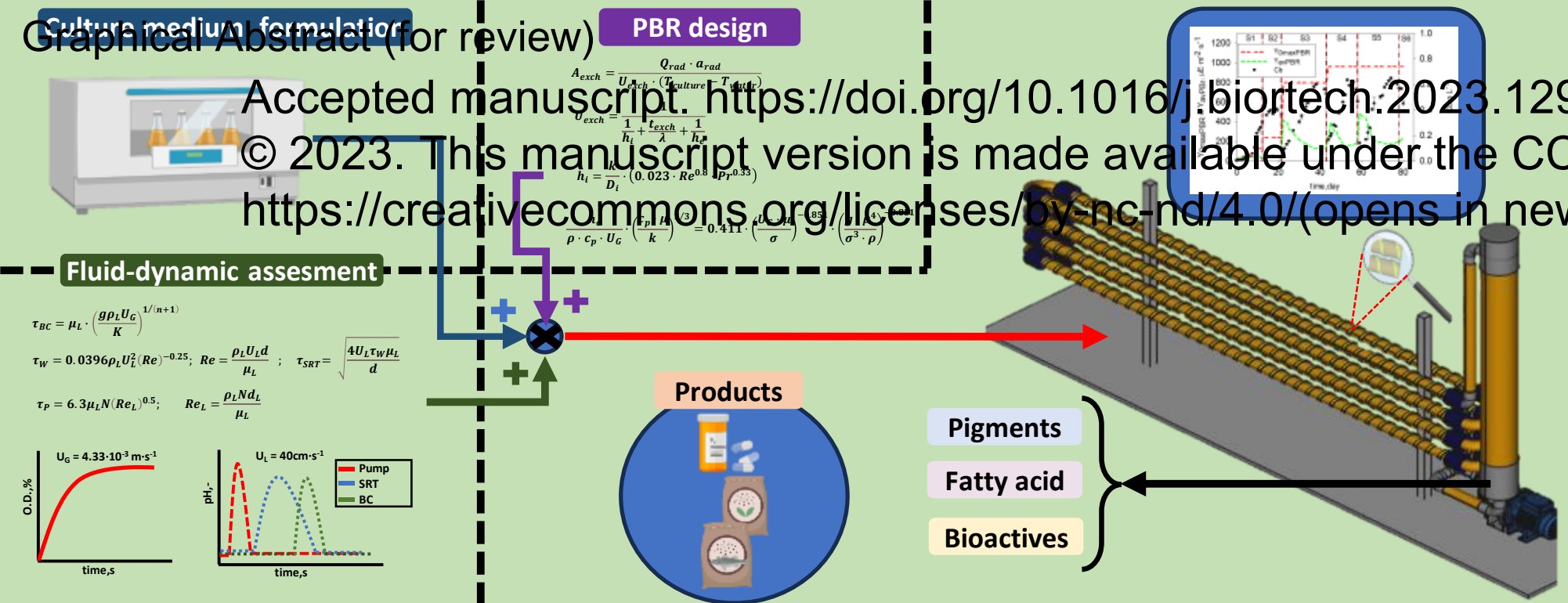

Abstract

Marine microalgae have potential to be low-cost raw materials. This depends on the exploitation of different biomass fractions for high-value products, including unique compounds. *Chrysochromulina rotalis*, an under-explored haptophyte with promising properties, was the focus of this study. For the first time, *C.* was successfully cultivated in an 80 L tubular photobioreactor, illuminated by an easy-to-use light-emitting-diode-based system. *C. rotalis* grew without certain trace elements and showed adaptability to different phosphorus sources, allowing a significant reduction in the N:P ratio without compromising biomass yield and productivity. The design features of the photobioreactor provided a protective environment that ensured consistent biomass production from this shear-sensitive microalgae. Carotenoid analysis showed fucoxanthin and its derivatives as major components, with essential fatty acids making up a significant proportion of the total. The study emphasizes the tubular photobioreactor's role in sustainable biomass production for biorefineries, with *C. rotalis* as a valuable bioactive feedstock.

Keywords: haptophyte; shear stress; carotenoid; fucoxanthin; biorefinery

1. Introduction

Marine microalgae show great potential as a valuable resource for generating large quantities of cost-effective basic commodities (i.e. biofuels) from biorefined microalgal biomass. However, the economic feasibility of microalgae-based bioprocesses conceived to obtain these commodities is currently dependent on the valorisation of different biomass fractions to produce exclusive and specialised products of high value, such as premium pigments or polyunsaturated fatty acids, which are known to be more expensive than more common and generic offerings (Sarkar et al., 2020; Vermuë et al., 2018). Furthermore, most of the microalgal specialty products are also present in most of the microalgae explored for this

purpose, so their potential differential value on the market may be lower than expected. In this respect, microalgae that are able to synthesise not only the typical reported commodities and specialties, but also other compounds or substances that, due to their uniqueness, have higher added value are needed. This is the case for bioactive microalgal compounds that exhibit a wide variety of functionalities and unique chemical structures, offering immense potential for applications in biomedicine, pharmacology, and agricultrure (O'Neill, 2020).

On this basis, haptophytes, a group of unicellular microalgae consisting of more than 350 characterised species, most of them marine, could be interesting candidates (Bashir et al., 2018; Leong et al., 2022; O'Neill, 2020; Seoane et al., 2009). Some of them belonging to the genera *Tisochrysis* and *Pavlova* are particularly valuable for aquaculture industries, serving as food enriched in essential lipids in diets for farmed fish and shellfish (Shah et al., 2018). However, the haptophytes of the genus *Chrysochromulina* are the only ones so far reported with the dormant potential to produce novel active metabolites with specific, undeveloped mechanisms of action (Hovde et al., 2015; John et al., 2002). Additionally, the genus *Chrysochromulina* is a producer of valuable compounds typical of microalgae-based bioprocesses or biorefineries (fucoxanthin and its derivatives, polyunsaturated fatty acids, with eicosapentaenoic acid (EPA) and docosahexaenoic acid (DHA) being predominant types, etc.) (González-Cardoso et al., 2023; Bigelow et al., 2013; Seoane et al., 2009).

Nevertheless, the main limitation observed in the aforementioned culture studies with the genus *Chrysochromulina* is the utilisation of extremely small culture scales for operation (less than 1.5 litres culture volume in the best case), specifically designed for genetic, ecology, or screening purposes. More studies are needed to assess the real value of *Chrysochromulina* as a feedstock for biorefinery. Manipulation of different abiotic stresses and environmental stresses through cultivation modes is mandatory to generate and / or increase the production of high-value biochemicals (Chen et al., 2017). Similarly, those best small-scale results should be taken to a proof of concept using bench- or pilot-scale photobioreactors (PBR). However, the implementation of entirely monoalgal cultivation in PBRs becomes essential, particularly

when the intended product is anticipated for use in both human and animal applications, and the producer alga requires environmental conditions that are not highly selective only for it.

In general, compact closed photobioreactors (PBRs) enable successful large-scale monoalgal cultures by preventing unwanted phytoplankton invaders (Molina-Grima et al., 2022; Sirohi et al., 2022). However, pneumatic agitation in PBRs can be detrimental to shear-sensitivity algal cells, severely restricting the attainable productivity (Sobczuk et al., 2006). For instance, attempts to culture the haptophyte *Isocrhysis galbana* in a closed tubular PBR with recirculation using a centrifugal pump were reported as unsuccessful (Michels et al., 2016). Additionally, the use of artificial illumination is recognised as suitable for the production of high-value microalgal compounds in PBRs (Ooms et al., 2016). Light emission diodes (LEDs) are replacing traditional artificial light sources for their energy and environmental advantages (Glemser et al., 2016). However, the potential for simple and low-cost LED-based illumination of tubular PBRs remains unexplored.

This work reports for the first time on the feasibility of culturing a commercial potentially marine haptophyte of the genus *Chrysochromulina* in a pilot-scale PBR using batch, fed-batch, and semicontinuous modes. The culture device is a custom-made 80 L tubular PBR driven by a centrifugal pump and illuminated by an easy-to-deploy LED-based system. The hydrodynamics of the PBR was evaluated mainly in terms of the shear stress tolerance of *Chrysochromulina*. Different concentrations and illumination regimes were tested. By adopting a two-dimensional diffuse incident light model, it was possible to estimate the average irradiance in the culture. Different culture medium formulations were assayed with the purpose of obtaining enhanced productivities of biomass and compounds, ruling out unnecessary trace metals. The assessment of maximum biomass productivity primarily relied on the daily mean absorbed volumetric photon flux. The analysis of harvested biomass involved evaluating carotenoid and fatty acid content.

2. Materials and methods

2.1. The microalga

The marine microalga *Chrysochromulina rotalis* BMCC18 (LT560338 – GenBank accession number), provided by the Basque Microalgae Culture Collection (Spain), was used. Inocula were grown and maintained in shake flasks under a 12:12 h light-dark cycle at 18 ± 2°C. The illumination was provided by multicolour light emitting diode strips (LED) with a power consumption of 19.2 $W \cdot m^{-1}$ (RGBW; Edison Opto Co., Taiwan) (López-Rosales et al., 2016), resulting in an average irradiance of 100 $\mu mol \cdot m^{-2} \cdot s^{-1}$ on the surface of the culture flasks. F/2 medium modified at a N/P molar ratio of 5, prepared using filter sterilised (0.22 µm Whatman GF/F 47 mm filters; Maidstone) brackish water at 30 psu, was used to grow the cultures unless otherwise specified. Brackish water was prepared by mixing Mediterranean seawater with freshwater.

2.2. Influence of the culture medium composition on growth

The effect of five different culture media on the growth of *Chrysochromulina rotalis* growth was evaluated. The culture media selected were the following: f/2, f/2-urea, K, K-PO_4, and L1(Se) (Andersen, 2005) (see Supplementary Materials). Multiple concentrations were evaluated by applying proportional multiplication to each of them (i.e., ×1, ×3 and ×6). The N:P ratio of the original f/2 formulation was reduced from 24 to 5 by increasing the phosphate-P concentration. In the f/2-urea medium, the nitrate as nitrogen source was replaced by urea. In the K-PO_4 medium, the phosphorus was added as phosphate. The L1(Se) medium consisted of L1 medium supplemented with selenium, an element that has been reported to promote the growth of haptophytes (Wehr and Brown, 1985). This experimental plan involved 15 batch culture experiments in total, each one conducted in duplicate.

Erlenmeyer flasks of 100 mL with a 50-mL filling volume without bubbling were used as culture vessels. The inoculum was taken from the mid-exponential growth phase and added to fresh medium at approximately 10% (v/v) until reaching a cell concentration of 3.37±0.41 $\times 10^5$ cells mL^{-1}. Cells were previously acclimated at the different formulations (see Supplementary Materials). The flasks were held on an incubator (Infors Multitron-HT, Switzerland), shaken continuously at 110 rpm at a temperature of 17 ± 1 °C. The cultures

were illuminated by an overhead bank of multicolour LEDs strips with a power consumption of 19.2 W·m^{-1} (RGBW; Edison Opto Co., Taiwan). rendering an average irradiance at the top surface of the flask of 120 µmol·m^{-2}·s^{-1}.

2.3. The LED-based tubular photobioreactor and its characterization

A custom-made vertical-fence tubular photobioreactor (tPBR) driven by centrifugal pump was designed and built for this study. A common tPBR basically consists of three interconnected parts: light collector, bubble column as degasser and culture pumping device. The light collector consisted of borosilicate glass tubes (Duran, Schott, Germany, 4.4 mm wall thickness and 50.4 mm internal diameter) vertically stacked as shown in the Figure 1. The tubes, connected by glass U-bends and plastic couplers (Schott, Germany), formed 8 loops of 2.5 m long with a total length of the receiver of 30 m. The illumination was provided by multicolour LEDs strips similar to those described in the previous section. The LED strips were placed in the light collector's tubes and the bubble column in a helical way with 7 cm of average nut pitch. A total of 7 m of LED strip per tube and 5 m in the bubble column were used. Both the tubes and the bubble column were lined with aluminium foil to prevent irradiance loss. A LED control system allowed for the flexibility to select any lighting schedule (López-Rosales et al., 2016). Thus, a sinusoidal (*Sns*) diel variation pattern of irradiance was implemented based on the equation provided by (López-Rosales et al., 2016):

$$[I_0(t)]_{SRT\ or\ BC} = \begin{cases} (I_{0max})_{SRT\ or\ BC} \cdot \sin\left(\pi \cdot \dfrac{t - t_{sr}}{t_{ss} - t_{sr}}\right) & if\ t_{sr} \le \mathrm{t} \le t_{ss} \\ 0 & otherwise \end{cases} \quad (1)$$

where I_{omax} is the maximum irradiance occurring at midday; t_{sr} is the time of sunrise; and t_{ss} is the time of sunset of the simulated solar cycle. Thus, for example, a L/D cycle of 12:12 means t_{sr}=6 h, t_{ss}=18 h, with a dark period of 12 h. Measurements of I_{omax} necessary for the Eq. (1), were conducted at various axial locations along the central axis of a light collector's tube and the bubble column, both filled only with brackish water. An average value of $(I_{omax})_{SRT}$ for the light collector and another for the bubble column $(I_{omax})_{BC}$ were used in Eq. (1). For the case of constant continuous lighting (i.e., 24:0 L/D cycle), eq. (1) is simplified to

$I_0(t)=I_{omax}$. Irradiance values were assessed with the aid of a spherical quantum sensor (Biospherical QSL 100; Biospherical Instruments Inc., San Diego, CA, USA).

The bubble column had two functions: degassing the dissolved photosynthetic oxygen and supplying carbon dioxide to the cells. It was constructed from transparent poly(methyl methacrylate) with a thickness of 3.3 mm, an internal diameter (d_C) of 0.14 m and 1.55 m in height from base to top. At the base of the bubble column, air injection was carried out using a 12 mm single-orifice sparger. The circulation of the broth through the light collector was carried out by a centrifugal pump (Kripsol KSE75, Sevilla, Spain) connected to a variable frequency drive that allowed modulating the circulation rate of the culture through the tubes. The total working volume of the tPBR was 82.2 L, with 26.79%, 72.50% and 0.71% of it corresponding to the bubble column, light collector, and centrifugal pump, respectively. The rate of circulation of the culture through the light collector's tubes was set to 40 cm s^{-1}. Inside the bubble column a stainless-steel coil heat exchanger through which temperature-controlled water at 10 ºC and at a flow rate of 28 L·min^{-1} was circulated from a chiller (HRS050-AF-20, SMC) with a centrifugal pump. The exchanger was sized as described elsewhere (Hikita et al., 1981; Tosun, 2007), considering that the major heat source comes from the lighting system. To calculate the necessary exchange area, a value for I_{omax} of 1000 µmol·s^{-1}·m^{-2} (= 218 W·m^{-2}) in both the light collector and bubble column was set. An air flow rate of 4 L·min^{-1} was used. At the conditions above described, a minimum exchange area of 0.25 m^2 was estimated. A safety margin was included, in such a way that the fixed exchange area was increased up to 0.4 m^2. The built heat exchanger consisted of 4 straight tubes interconnected, each 1.25 m long and 16 mm in external diameter.

At the mean circulation velocity in light collector's tubes (U_L) of 40 cm s^{-1}, the mixing time, residence time, circulation time and the linear velocity of the liquid in different zones of the tPBR were estimated by using the tracer method as previously reported (Sánchez Mirón et al., 2004). Briefly, a pulse of 15 mL of a 10% w/v HCl solution were instantaneously injected into the cavity of the centrifugal pump. Three pH electrodes were utilized to monitor the variation in pH over time. The electrodes (HI1110B, Hanna, EEUU) connected to transmitters

(HI8711, Hanna, EEUU) were located at the inlet and outlet of the light collector, and at the bottom of the bubble column, just before the entrance to the centrifugal pump. The pH data were recorded digitally with a data acquisition card LabJack U12 (LabJack®, 2004) and the DaqFactory software (AzeoTech Inc, AK, EEUU). By employing the dynamic degassing method, the average overall volumetric mass transfer coefficient (K_La) was determined to be 0.006 s^{-1} (Mirón et al., 2000). The rough estimate of the shear stress profile in the tPBR was performed according to a previous study (Chisti, 2009). Thus, the mean shear stress in the degasser (i.e., the bubble column) (τ_{BC}), the wall shear stress in the light collector tubes (τ_W), and the average shear stress in the light collector tubes (τ_{SRT}) were 0.24 Pa (equivalent to a shear rate γ_{BC} of 183 s^{-1}), 0.58 Pa, and 0.16 Pa, respectively (see Suplementary material). Regarding the centrifugal pump, a local shear stress (τ_P) of 573.6 Pa was estimated for the culture adjacent to the rotating impeller. The mean residence time (t_R) in each of the three sections of the tPBR was estimated as a function of the mean circulation time (t_C) as reported previously for airlift photobioreactors (Contreras et al., 1999) (see Suplementary material): $(t_R)_{BC}$ = 27.79 s for the bubble column (degasser), $(t_R)_{SRT}$=76.96 s for the light collector, and $(t_R)_P$=0.25 s for the pump. The average shear stress (τ_{PBR}) to which the cells were exposed in the tPBR was calculated as follows:

$$\tau_{PBR} = \frac{\tau_{BC} \cdot (t_R)_{BC} + \tau_{SRT} \cdot (t_R)_{SRT} + \tau_P \cdot (t_R)_P}{t_C} \quad (2)$$

its value being 1.6 Pa, equivalent to a mean shear rate (γ_{PBR}) of 1214 s^{-1}. The minimum sizes of the fluid microeddies in the bubble column and the light collector were estimated as proposed elsewhere (Chisti, 2009).

2.4. Cultivation in the tubular photobioreactor

The photoautotrophic growth of *C. rotalis* was investigated in the tPBR. Before use, both the photobioreactor and the brackish water for cultivation were jointly sterilized using a sodium hypochlorite solution, followed by neutralization with sodium thiosulfate, as previously explained (López-Rosales et al., 2016). The accumulation of dissolved

photosynthetic oxygen in the tPBR was monitored by measuring the dissolved oxygen (DO) concentration at the light collector outlet and at the bubble column. The culture temperature was controlled at 18±1 ºC. The heat exchanger displaced a volume of 1.1 L. pH control was maintained at pH 8.05 through the automated injection of carbon dioxide, as required.

The medium formulation that provided the best growth results in the assays described in Section 2.2 was selected for cultivation. Inoculum was then acclimated to selected medium under the environmental conditions described in Section 2.1. At the outset of the experiment, a batch culture phase was initiated by inoculating 15 L of an inoculum, comprising algal cells in the late exponential growth phase, into 67.2 L of Kx6 medium. The biomass concentration in the freshly inoculated tPBR was approximately 6 ± 0.1 $mg \cdot L^{-1}$ (equivalent to $(1.9 \pm 0.1) \times 10^5$ cells mL^{-1}). Once the steady state of growth was reached, several experimental sets were implemented sequentially combining illumination regime, nutrients concentration and culture mode. The entire operational plan, which is meticulously set out in (Table 1), began with a gradual process of acclimatization of the cells from the inoculum conditions to those prevailing in the tPBR using batch culture mode and increasing the irradiance level over time (set 1 in Table 1).

In fed-batch mode, concentrated medium stocks were added on days 13 and 18 of culture until initial concentrations of nitrates and phosphates were adjusted according to Table 1. To achieve this, a one-liter portion of the culture was substituted with an equal volume containing the required nutrient stock, equivalent to 82.2 L of the medium employed. While nitrogen was added in the amount necessary to return its culture concentration to the initial value, phosphorus was supplemented to achieve a culture concentration according to a specific initial N/P ratio (Table 1). The rest of the nutrients were supplemented in the same proportion than phosphorus. When the fed-batch mode ceased to improve biomass production, a semicontinuous mode (Sets 3-5) was explored by adopting a strategy similar to one previously reported (Molina-Miras et al., 2018a). If sufficient nutrients were present in the culture, the light availability to cells was increased by extending the illuminated period (D) within the 24 h L/D cycle until even the setting continuous irradiance at a constant level (24:0 in Table 1).

Finally, Set 6 consisted of applying hyposaline stress via a sudden change in salinity from 30 to 5 psu. For that, a 70 L culture volume was withdrawn and centrifugated. An equivalent volume was replenished with 2 psu brackish water, enriched with nutrients stock solutions, ensuring that the final nutrient concentrations in the entire culture volume (=82.2 L) reached 10% of the medium formulation. The cell pellet obtained was resuspended in 1 L of 30 psu brackish water and then added to tPBR. The culture was maintained in batch mode for 48 hours before being under centrifuged to harvest the biomass.

The photobioreactor was subjected to various illumination regimes during operation as given by Eq. (1) by varying the I_{omax} and L/D cycle as described in Table 1. The average irradiance inside the whole culture, $I_{avPBR}(t)$, a time t was estimated as reported for this type of LED illumination elsewhere (López-Rosales et al., 2016):

$$I_{avPBR}(t) = \frac{V_{SRT}(1-\epsilon_{SRT})}{V_{PBR}(1-\epsilon_{PBR})} \cdot I_{avSRT}(t) + \frac{V_{BC}(1-\epsilon_{BC})}{V_{PBR}(1-\epsilon_{PBR})} \cdot I_{avBC}(t) \quad (3)$$

where $I_{avBC}(t)$ and $I_{avSRT}(t)$ are the average irradiances inside the culture residing in the bubble column and light collector's tubes, respectively, given by

$$I_{avSRT\ or\ BC}(t) = \frac{2 \cdot [I_o(t)]_{SRT\ or\ BC}}{R^2 \cdot \pi} \cdot \int_0^R \int_0^\pi e^{-\omega(t)\cdot(r\cdot cos\phi + \sqrt{(R^2 - r^2 \cdot sin^2\phi)})} \cdot r \cdot d\phi \cdot dr \quad (4)$$

where R is the internal radius of the bubble column or that of the light collector's tube, r is the radial position in both, ϕ is the angle at which the incident light beam penetrates and $\omega(t)$ the mean effective attenuation coefficient of the microalgal suspension, computed across the PAR wavelengths. The $\omega(t)$ value was estimated from the following equation:

$$\omega(t) = K_a(t) \cdot C_b(t) \quad (5)$$

In the above equation, $C_b(t)$ is the biomass concentration (g m^{-3}) and $K_a(t)$ (m^2 g^{-1}) is the effective light attenuation across biomass over the PAR wavelengths at t time. The $K_a(t)$ value was determined spectrophotometrically using the following equation (Acién Fernández et al., 1997):

$$K_a(t) = \frac{1}{C_b(t) \cdot p} \cdot \frac{\int_{400}^{700} Abs(\lambda, t) \cdot d\lambda}{\Delta\lambda} \quad (6)$$

where $Abs(\lambda, t)$ is the light absorption of the culture at the wavelength of λ a time *t*. $Abs(\lambda)$ was measured in a multi-well plate reader (SynergyMx, BioTek® Instruments Inc., USA). The optical path of each well (p) was 10.9×10^{-3} m. The daily mean I_{av} (referred to as Y_{av}) was calculated as follows, according to López-Rosales et al. (2016):

$$Y_{avPBR} = \frac{1}{24} \cdot \int_{t_{sr}}^{t_{ss}} I_{avPBR}(t) \tag{7}$$

The photon flux absorbed in the entire culture volume (F_{vol} (t), $\mu E \cdot m^{-3} \cdot s^{-1}$) and the daily mean of the F_{vol} (i.e. Γ_{av}), were estimated using the following equations (López Rosales et al., 2016):

$$F_{vol} = I_{avPBR}(t) \cdot \omega(t) \tag{8}$$

$$\Gamma_{av} = \frac{\int_{t_{sr}}^{t_{ss}} F_{vol}(t) \cdot dt}{24} \tag{9}$$

The upper limit of the photon flux that the culture can potentially absorb (denoted F_{max}) was determined by taking the limit of Eq. (8) as the extinction coefficient ($\omega(t)$) approaches infinity, resulting in the following expression:

$$F_{max} = \frac{2 \cdot [I_0(t)]_{SRT\ or\ BC}}{R \cdot \pi} \tag{10}$$

The calculation for daily mean F_{max} (Γ_{max}) during the daily illuminated period is as follows:

$$\Gamma_{max} = \frac{\int_{t_{sr}}^{t_{ss}} F_{max}(t) \cdot dt}{24} \tag{11}$$

2.5. Kinetic parameters

Productivities of biomass (P_b) and microalgal compounds (P_p) were respectively calculated as follows:

$$P_b = \frac{C_{bf} - C_{bi}}{t_f - t_i}; \qquad P_p = P_b \cdot X \tag{12}$$

where the subscripts i and f refer to the start and end of each time interval between two consecutive measurements; and X is the weight fraction of compounds in the dried microalgal biomass. The maximum daily biomass productivity (P_{bmax}) was selected as the maximum value of P_b for each set.

2.6 Analytical measurements

Samples of the order of millilitres were withdrawn from the different culture experiments and then centrifuged (benchtop centrifuge, model SIGMA 4-15C, 6000× g, 5 min). The resulting pellets were washed twice with 0.5 M ammonium bicarbonate solution and then freeze-dried (Cryodos 50, Telstar). Dry biomass and supernatants were immediately analyzed or stored frozen at -22°C until its later use. Culture volumes harvested from tPBR operated in both semi-continuous and hyposaline stress modes were centrifuged in continuous mode (RINA, model 100M/200SM, Spain) at 1000 ×g fed with a broth flow rate of 15 $L \cdot h^{-1}$. The resulting microalgal sludges (retentates) were also freeze-dried.

The assessment of extracellular lactate dehydrogenase (LDH) levels served as an indicator of lytic cell death induced by hydrodynamic and mechanical stresses affecting cellular membranes. Elevated LDH in culture supernatants indicated potential cell lysis. LDH measurements were reported in activity units (U), following established protocols Gallardo-Rodríguez et al., 2015; Gallardo-Rodríguez et al., 2016; López-Rosales et al., 2018). Shortly, culture samples were taken at the starting and the end of each set and gently centrifuged. Subsequently, LDH levels of supernatants (LDH_S, U mL^{-1}) and harvested intact cells were measured. The latter measurement allowed to determine intracellular LDH level per cell (LDH_{cell}, U $cell^{-1}$). The difference between the LDH_S measured at the beginning and end of each set allowed the determination of cumulative LDH concentrations in the culture supernatant (ΔLDH_S). For the purpose of comparison, LDH_{cell} and LDH_S were also determined in a static control culture conducted in flasks under the same environmental conditions as the inoculum described in Section 2.1.

Using samples withdrawn throughout the cultures, a biomass concentration calibration curve was obtained using the optical density at 720nm (OD720) and the dry biomass (Molina-Miras et al., 2018b): Cb (g/L) = $0.5905 \cdot OD_{720}$ (r^2 = 0.915; n = 25). The following other determinations were carried out as previously reported: (i) maximum photosynthetic efficiency of photosystem II (*Fv/Fm*) in cells (López-Rosales et al., 2016); (ii)

total phosphorus and nitrate-N in supernatants (Molina-Miras et al., 2018a); (iii) carotenoid content and profile using an HPLC photodiode array detector (Cerón-García et al., 2018); (iv) fatty acid (FA) content and profile by direct transesterification and gas chromatography (Molina-Miras et al., 2018a); (v) hemolytic activity of the methanolic extracts from biomass (Molina-Miras et al., 2018b), based on values of EC_{50} for saponin relative to EC_{50} for *C. rotalis*, named equivalent saponin potency, ESP, pg saponin per μg of biomass methanolic extract giving 50% hemolysis; (vi) in vitro anticancer activity assays (Abreu et al., 2019) for three crude extracts obtained from *C. rotalis* biomass samples harvested at the end of each set (Table 1). Four human tumor cell lines were used: A549 (lung carcinoma), HT-29 (colon adenocarcinoma), MDA-MB-231 (breast adenocarcinoma), and PSN-1 (pancreas adenocarcinoma). The crude extracts at point (vii) were obtained with 100% methanol. For comparison purposes, ESP was also determined in the biomass of the microalgae *Isochrysis galbana* and *Nannochloropsis gaditana* widely used in aquaculture (Shah et al., 2018), and *Amphidinium carterae* characterized by producing amphidinols, substances with antiproliferative and hemolytic activity (Abreu et al., 2019). All measurements were performed in duplicate and the average value was used.

2.7. Statistical analysis

The experimental outcomes were presented as mean values derived from two independent experiments, along with their corresponding standard deviations.. The normality and homogeneity tests were performed using the Kolmogorov-Smirnov and Levene tests, respectively. Significant difference analysis with a one-way and multi-way analysis of variance (ANOVA) test were performed. Statistical data analyses were conducted using the Statgraphics Centurion XVII (version 17.2.04) statistical software (2014, Statpoint Technologies, Inc., Warrenton, VA).

3. Results and discussion

3.1 Selection of culture medium

Before investigating the potential of *C. rotalis* to be cultivated in the pump-driven tPBR, a brief study was carried out to select a suitable culture medium. The f/2 medium has been cited the most times in the literature for the genus *Chrysochromulina*; the rest has occasionally been used in haptophytes. Each formulation was tested at three levels of nutrient concentration (×1, ×3 and ×6; see Section 2.2 above). The differences between the culture media were significant according to the formulation basis, i.e. f/2, K and L1. Within each formulation basis, the differences were mainly due to the type of nitrogen source (nitrate versus urea in f/2) and type of phosphorous source (inorganic phosphate versus organic phosphate in K). L1-Se was characterized by a high concentration of Se and the presence of other trace elements such as Ni, V, and Cr.

Measurements of maximum biomass concentration (C_{bmax}) and productivity (P_{bmax}) were determined for all the experiments. Urea-related toxicity was observed in the f/2-urea medium formulations because cells did not survive sub-cultivations. Thus, while *C rotalis* was unable to acclimate to the minimum initial urea concentration assayed of 882 µM, it did for the rest of media. In order to examine the influence of the two factors under consideration (medium and concentration level) on C_{bmax} and P_{bmax}, a two-way ANOVA was performed, but excluding results from f/2-urea medium. Only the concentration level had a statistically significant effect on C_{bmax} ($p=0.000$; F-ratio= 41.98) and P_{bmax} ($p = 0.009$; F-ratio = 10.54). As can be seen in Figures 2A,B, C_{bmax} linearly increased with the nutrient concentration in the medium, whereas P_{bmax} began to plateau at ×3 concentration level. This response indicated that the biomass yield of the cultures was mainly controlled by the availability of dissolved nutrients in the medium, inorganic carbon and light being supplied in enough amounts. However, the inorganic carbon (diffusive transport of CO_2 from the air across the culture-free surface) and light supply rates appeared to limit the growth rate from the concentration level x3.

The growth response of *C. rotalis* described above is not unexpected given the highly interspecific observations previously reported for the haptophyte taxon *Chrysochromulina* when cultured under different sources of nitrogen, such as nitrate, urea, or ammonium

(Rhodes and Burke, 1996), although no study was found in which urea above 800 µM in culture medium was toxic for *Chrysochromulina*. It is very likely that the level of tolerance to urea is also species dependent. Of particular interest is the effect of selenium (Se). Although no significant differences in the growth rate of several *Chrysochromulina* species were observed between cultures supplemented with Se compared to those without selenium (Rhodes and Burke, 1996), Se greatly enhanced the growth and long-term maintenance of *C. breviturrita* (Wehr and Brown, 1985).

In this study, it was demonstrated that *C. rotalis* could grow without the trace elements Ni, V, and Cr (L1-Se medium), the culture medium should not contain urea as a nitrogen source (f/2-urea medium) and the phosphorus source could be either $NaH_2PO_4 \cdot H_2O$ or sodium glycerophosphate. Although *C. rotalis* seemed to lack a crucial dependence on Se (f/2 did not contain Se), this trace element has been documented to mitigate the oxidative damage to photosynthesis, suppress lipid peroxidation, and regulate intracellular reactive oxygen species or have a relevant role in the production of secondary metabolites such as toxins by some microalgae (Borowitzka, 2018). Additionally, the formulations of the media used (see Supplementary Materials) presented three different molar N:P ratios (nutrient-N content was fixed with the P content adjusted accordingly): 5:1 (f/2 medium), 22:1 (L1-Se medium) and 88:1 (K and K-PO_4 media). It is evident that a N:P ratio below 88:1 was in surplus phosphorous for biomass production and therefore this nutrient could be reduced at least up to 88:1 without compromising biomass yield and productivity at any concentration level assayed. The use of high N:P ratios in chemically-defined culture media can offer considerable savings and improve the sustainability of microalgae-based bioprocess (Mayers et al., 2014), and may also favor the synthesis of secondary metabolites (Van de Waal et al., 2014). As a result, the medium K at the nutrient concentration ×6 was selected for its usage in the culture of *C. rotalis* in the tPBR. K medium has been widely used in the bioprospecting of marine microalgae for the search of novel bioactive compounds (de Vera et al., 2018).

3.2. Shear stress tolerance in the tubular photobioreactor

The capability of *C. rotalis* to grow in a tubular PBR in which the culture was recirculated using a centrifugal pump was assessed. There was no evidence that the average shear stress level developed in the tPBR negatively influenced the cell growth.

Cell lysis was quantified using cumulative LDH concentrations (ΔLDH_S) in the culture supernatant (see Supplementary Material). This measurement served as a proxy to assess shear-induced damage. LDH_S accumulation was observed in all sets and the values of ΔLDH_S varied depending on the cell concentration increase of each set, ranging from 103 $\times 10^{-6}$ U mL^{-1} for Set 2 to 688 $\times 10^{-6}$ U mL^{-1} for Set 3. To estimate the total number of cumulative cells that might have been lysed, ΔLDH_S was divided by the intracellular LDH level (LDH_{cell}) measured at the end of each set, resulting in an equivalent number of lysed cells. Across all sets, this calculation yielded a consistent range of between 1.2% and 3.1% of the total cell concentration, which aligns with the percentages obtained for cells grown in static (i.e., non-shake) flasks. Furthermore, the average intracellular LDH value for all sets in the tPBR ((1.54 ± 0.03)$\times 10^{-9}$ U $cell^{-1}$) was not significantly different from that obtained from the static flasks ((1.51 ± 0.02)$\times 10^{-9}$ U $cell^{-1}$). Compared to cells grown in a static control culture, the morphology and flagella of cells grown in the tPBR were preserved, although with lesser motility. Taken together, these results indicate the absence of shear-induced damage to cells exposed to the hydrodynamics of the tPBR when operated at a 40 cm s^{-1} U_L.

Studies on shear stress tolerance of haptophytes are limited (Wang and Lan, 2018). Under short-term exposure to Couette flow, a shear stress threshold of 5.4 Pa was reported for *I. galbana* (Michels et al., 2016). However, *I. galbana* did not endure short-term cultivation in a tubular photobioreactor operated at a culture circulation rate in the tubes of 0.37 m s^{-1}. This pumping speed lead a rough average shear stress for the whole tPBR (τ_{PBR}) of 0.371 Pa (this figure was obtained applying Eq. 9 to data reported in (Michels et al., 2016); more than an order of magnitude below the threshold value endured under Couette flow. This discrepancy was attributed to the effect of the passage frequency of the cells by the pump (Michels et al., 2016), since the main contributor to τ_{PBR} was the shear stress developed in the region of the

centrifugal pump (τ_p) with an estimated value of 26 Pa (Michels et al., 2016), compared to the degasser ($\tau_{BC} = 0.54$ Pa) and light collector's tubes ($\tau_{SRT} = 0.19$ Pa).

In contrast, in our study, *C. rotalis* grew in absence of shear-associated damage in the tPBR operated at a pumping speed of 2.83 $m^3 h^{-1}$ (equivalent to a U_L of 0.40 m s^{-1}). This pumping speed lead a τ_{PBR} value of 1.6 Pa, averaged from the following local values of shear stress (Eq. 9): $\tau_{BC} = 0.24$ Pa, $\tau_{SRT} = 0.16$ Pa and $\tau_P = 573.6$ Pa. The value of τ_P was 4.5-fold higher than that for *I galbana*. Therefore, *C rotalis* showed tolerance to moderate average shear stress compared to most microalgae reported in the literature (Wang and Lan, 2018).

The high value of τ_p experienced by the cells of *C rotalis* as they passed through the centrifugal pump was about five orders of magnitude greater than the shear stresses experienced by the cells in the degasser or light collector. It is unlikely that the cells could withstand continued shear stress of that magnitude. However, any infinitesimal fluid element resided in the centrifugal pump only 0.24 s into the cycle time (t_c=104 s). It is evident that the combination of low passage frequency (inverse of t_c) and a tiny proportion of cycle time (0.24 s) in which cells were exposed to acute shear stress was insufficient to inhibit growth or to irreversibly damage *C. rotalis*. This is supported by previous experiences with dinoflagellates, very shear-sensitive microalgae, capable of enduring enormous acute single hydrodynamic forces when applied over time intervals below 1 s (Gallardo-Rodríguez et al., 2015).

The design and operation of tPBRs also had to comply with other restrictions. In this respect, the air flow rate in the bubble column (0.198 vvmin) and U_L in the tubes were such that the corresponding minimum sizes of the fluid microeddies (λ_{BC}= 83 μm and λ_{SRT}= 102.7 μm, respectively) exceeded that of the algal cells (5.83±1.41 μm), so that turbulence-related damage in both degasser and light collector was prevented. Regarding the light collector, the U_L value also determines the maximum permissible length of the continuous run tube (L) established by inhibition of growth by oxygen or cell damage by photooxidation (Molina et al., 2001). Both are largely responsible for dissolved oxygen values at the outlet of light collector tube and the volumetric rate of photosynthetic oxygen generation by in the tube as reported elsewhere (Molina et al., 2001). At 0.4 m s^{-1} U_L, the fixed length of the continuous

run tube (L= 30 m) avoided in excess accumulation of photosynthetic dissolved oxygen; at most $[O_2]_{out}$ values of 150% on air saturation were recorded. Consequently, the appearance of inhibition or photooxidation was improbable, even more so when the oxygen concentration at the entrance, $[O_2]_{in}$, of the light collector tube was close to the air saturation value. The latter evidenced a suitable capability of the degasser system for stripping oxygen. The design of bubble column head zone allowed flexibility for stripping (see Fig. 1). Thus, the inlet into the bubble column of the culture broth from the light collector could be made to contact the culture residing in the bubble column in two ways, depending on whether the level of the broth in the bubble column was below or above the inlet. Under the first option, a waterfall was generated that improved degassing, at the cost of increasing the number of bubbles inside the broth due to atmospheric air entrapment. The risk that the centrifugal pump will recirculate bubbles to the collector was greater the higher the difference in height. Under the second option, this risk decreases but the degassing capacity also decreases. In the culture experiment, a difference in height of 5 cm allowed almost complete separation of the gas from the culture, before the broth was recirculated in the light collector.

Two critical velocities of fluid circulation through the light collector tubes can be derived from the above analysis: the one, $(U_L)_{DO}$, below which allows the accumulation of oxygen at inhibitory levels for growth and the one, $(U_L)_{SS}$, above which the shear stresses that originated in different parts of the tPBR could be detrimental to cells. In line with this approach, a cell suspension with a density of 11×10^6 cells mL^{-1} and a biomass concentration of 0.345 g/L, obtained in the PBR under Set 4 conditions (as shown in Table 1), was subjected to an increase in the fluid circulation rate (U_L) from 40 cm s^{-1} to an unusually high 80 cm s^{-1}, which deviates from conventional practice in tubular photobioreactors. The biomass concentration began to decline within hours of the step change in U_L. After 2.5 days, virtually all the cells were lysed, with the culture supernatant having a final LDH_S value of almost 31 times the initial one, equivalent to a lysed cell concentration of around 10×10^6 cell mL^{-1}. At 80 cm s^{-1}, the occurrence of turbulence-induced damage in the light collector could be ruled out, since the sizes of fluid microeddies (λ_{SRT}= 63.771 μm) surpassed those of the algal cells.

Consequently, the local shear stress level within the centrifugal pump (τ_P =1234 Pa), needed to propel the fluid through the tubes of the light collector at 80 cm s^{-1}, seemed to be the primary source of cell damage. This observation implies that the critical $(U_L)_{SS}$ value, detrimental to cell integrity, should fall within the range of 40 to 80 cm s^{-1}.

However, the appearance of biofouling in tubular photobioreactors is a common phenomenon rarely reported that points to a new restriction in the selection of U_L not considered so far in the literature. The formation of biofouling in tubular PBRs is a complex process caused by the physicochemical interactions between cells, extracellular organic substances secreted by microalgae, and culture medium components with the PBR surfaces in contact with the broth. At the nanometer scale near the wall, the cell experiences a range of forces, including attractive forces, lift forces and drag forces parallel to the surface (Zeriouh et al., 2017). The overall net force resulting from this force balance will determine the ease of cell adhesion. The drag forces arise from the wall shear stress (τ_w=0.58 Pa, see Eq. 3), while the lift forces stem from the fluid velocity gradient close to the surface. Typically, the drag forces are significantly higher than the lift forces. Both are detachment forces that depend on U_L. Therefore, even knowing that the formation of biofouling is inevitable, there will be a critical flow velocity, $(U_L)_{BF}$, above which the net resultant force will allow cell adhesion to be hindered. The selection of $(U_L)_{BF}$ is not an easy process because once the conditioning film is formed on the PBR walls, the surface properties change over the course of cultivation and thus the direction of the resultant net force becomes more attractive. As a result, $(U_L)_{BF}$ should be increased progressively to reverse this unwanted effect. This procedure has two restrictions. $(U_L)_{BF}$ would always have to be lower than $(U_L)_{SS}$. On the other hand, the increase in $(U_L)_{BF}$ may lead to the preferential selection of cells that possess a greater resistance to detachment, ultimately resulting in the formation of very sticky and persistent biofilms. This analysis suggests that the selection of U_L implies considering the existence of $(U_L)_{DO}$, $(U_L)_{SS}$ and $(U_L)_{BF}$ and its effect on light availability for cells. The U_L value of 40 cm s^{-1} chosen to culture *C. rotalis* in the tPBR seemed to satisfy that criterium. On the contrary, intense biofouling formation was documented for an outdoor

tubular PBR operated at 0.40 m s^{-1} where *Nannochloropsis gaditana* was grown (Zeriouh et al., 2017). Interestingly, biofouling was also reported for cultivation of *Tetraselmis suecica* in an indoor tubular PBR operated at pumping speeds detrimental for cells (Michels et al., 2016).

Although the above assessment about the shear stress tolerance of microalgae in a typical tPBR serves as a rule of thumb for comparing results reported in literature, the interaction of cells with hydrodynamics developed in a tPBR is a complex matter when it is intended to operate near the shear stress regime tolerable by cells. The shear stress field developed in a tPBR is heterogeneous, with local shear stresses differing by several orders of magnitude. The cells during their movement through that shear stresses field experience a history of stress. Except for exceptional situations in which cells may pass through lethal stress zones that produce instant lysis, commonly cells do not respond instantly to growth inhibitory shear stresses, but rather to the experienced shear stress history (Gallardo-Rodríguez et al., 2016). Computational fluid dynamics modeling of photobioreactors could be a very useful tool to fine-tune the design and operating conditions of tPBR (Ranganathan et al., 2022).

3.3. Culture experiment and monitoring in the tubular photobioreactor

Figures 2C,D shows a representative culture profile of the tPBR according to the strategy shown in Table 1. The F_v/F_m value exhibited consistent stability over the culture period with an average of 0.462 ± 0.091, signifying the continued presence of thriving cells throughout the culture period. Set 1 portrayed a progressive rise in the maximum daily mean irradiance $(Y_{av})_{max}$ delivered to the tPBR in batch culture mode. The primary objective of this set was to promote acclimation of the inoculum cells to the prevailing conditions within the tPBR, effectively preventing potential photoinhibition. The increase in $(Y_{av})_{max}$ from 25 to 127 µE m^{-2} s^{-1} resulted in a corresponding increase in biomass concentration from 6.6 10^{-3} to 0.306 g L^{-1}, respectively. However, the average irradiance experienced by the cells (Y_{av}), considering mutual shading, remained relatively low, ranging from 24 to 37 µE m^{-2} s^{-1}. This suggests that cell growth was limited by light availability, consistent with findings reported for

various species of the genus *Chrysochromulina* grown in 10-mL optically thin cultures. These studies demonstrated that the growth of these species was light-limited below a daily average irradiance of 150 µE m^{-2} s^{-1} (no tests were reported above this threshold) (Seoane et al., 2009).

A slowdown in growth was observed in set 1 after 13 days of cultivation (Fig. 2C). Upon examining Fig. 2D, it became apparent that rapid depletion of dissolved phosphate in the supernatant was among the primary contributing factors, along with limited light availability. In contrast, nitrate-N remained in excess during this period. To confirm this hypothesis, the culture was supplemented with phosphate, increasing both its concentration to 251 µM on day 13 (as indicated in Table 1 for set 2, fed-batch mode) and $(Y_{av})_{max}$ to 238 µE m^{-2} s^{-1}. These adjustments also involved reducing the N/P ratio to 16:1. Growth acceleration was observed until it ceased on day 16 (Fig. 2C), coinciding with complete phosphate depletion (Fig. 2D). Despite the addition of phosphate to the culture on day 19, while keeping the N/P ratio constant at 16:1, all available phosphate was again depleted without any noticeable increase in biomass concentration after four days in set 2. This, combined with a Y_{av} value of 60 µE m^{-2} s^{-1}, indicated a growth limitation resulting from the scarcity of both nutrients.

To explore alternative approaches, from day 22, the culture was transitioned into a semi-continuous mode. This involved periodically removing a fraction of the volume of the culture and replacing it with nutrient-rich medium to restore the initial concentrations specified in Table 1 (set 3). Furthermore, $(Y_{av})_{max}$ was increased to 800 µE m^{-2} s^{-1}, allowing for enhanced light availability in the culture. This first semi-continuous culture ended on day 44, after three days in stationary phase (Figure 2C). During this period, the maximum biomass concentration achieved was 0.602 g L^{-1}, resulting in a net biomass yield of 0.512 g L^{-1}. Although nutrients were available in excess (Fig. 2D), Y_{av} decreased from 417 µE m^{-2} s^{-1} at the beginning of the culture (C_b=0.09 g L^{-1}) to 131 µE m^{-2} s^{-1}, indicating light-limited growth. Subsequently, from day 44 to day 78, two additional semi-continuous cultures (sets 4 and 5) were performed under continuous illumination at an increased $(Y_{av})_{max}$ of 960 µE m^{-2} s^{-1}. The maximum biomass yield attained was slightly higher in these sets, but reached in a shorter time, compared to set 2. The nutrients, including the available irradiance, remained in excess

throughout both sets, and Y_{av} never dropping below 150 µE m^{-2} s^{-1}. The observed pattern in the fluctuation of Y_{av} aligns with typical trends seen in semi-continuous cultivation, as extensively described in previous studies (Molina-Miras et al., 2018a; Molina-Miras et al., 2018b). Notably, the stationary phases observed in the cultures were relatively brief, characterised by a rapid decline. The specific cause of this phenomenon remains unknown, although possible explanations such as deficiencies in trace elements within the culture medium or the accumulation of growth-inhibiting metabolites are hypothesised. Further research will be required to gain a deeper understanding of this observation. Regarding the application of hyposaline stress in set 6, the primary objective was not to monitor kinetic parameters, but rather to observe the potential elicitation of compounds of interest. This aspect will be discussed in the following sections.

Figure 2E illustrates the relationship between Γ_{av} (daily mean absorbed volumetric photon flux) and the P_{bmax} values for sets 1-5. The Γ_{av} values closely align with Γ_{max} of each set, indicating efficient photon absorption by the culture. These results suggest the presence of dark zones within the tubes and bubble column as reported in an earlier study conducted in a bubble column photobioreactor (López-Rosales et al., 2016), where total incident photon flux was absorbed, leading to a kinetic regime (i.e. the regulation of the growth rate is governed by the metabolic assimilation of energy). However, the assessment does not consider the rate at which fluid exchanges between the inner dark and outer well-illuminated culture zones, which directly influences the light-dark cycle of the cells. Modulating the liquid pumping and aeration rates would allow for control over fluid interchange through U_L, but consider the existence of $(U_L)_{DO}$, $(U_L)_{SS}$ and $(U_L)_{BF}$ and its potential effect on cells. Although the occurrence of a dark zone is unavoidable in tubular PBRs with large diameter tubes and bubble column degassers, its effects can be mitigated by optimising aeration and liquid flow rates (López-Rosales et al., 2016).

Overall, the designed tubular reactor offered an effective solution to ensure a consistent and reliable supply of biomass from a shear-sensitive microalga. By tuning its engineered features, a protective environment was found that minimises shear stress and

maintains the integrity of the microalgae culture. This research underscores the practical importance of the tubular reactor in cultivating shear-sensitive microalgae, contributing to advances in sustainable biomass production for scientific and industrial applications.

3.4 Compounds from Chrysochromulina: characterization and analysis

González-Cardoso et al. (2023) proposed a sequential partitioning method to isolate bioactive compounds from *Chrysochromulina rotalis* using environmentally friendly solvents and a polarity gradient (González-Cardoso et al., 2023). The study reported the main fatty acids and carotenoids identified in the biomass harvested in set 4. In the work presented here, the biomasses harvested in the rest of the sets were also characterised, presenting the similar profiles in carotenoids and fatty acids as in set 4. Therefore, *C. rotalis* exhibited in all sets a consistent presence of primary carotenoids, including fucoxanthin, diadinoxanthin, diatoxanthin, nonpolar chlorophyll, and β-carotene. In addition, minor carotenoids such as 19'-butanoyloxyfucoxanthin and 4-keto-19'-hexanoyloxyfucoxanthin were observed. In particular, fucoxanthin and its derivatives (4-keto-hex-fucoxanthin and Hex-fucoxanthin) accounted for approximately 40.3±7.7% of the total carotenoid content, while diatoxanthin represented nearly 18.7±6.7% of the total. The majority of fatty acids present in this microalga consist of saturated or monounsaturated forms, accounting for around 67.5±7.7% of total fatty acids. Polyunsaturated fatty acids (PUFAs), specifically stearidonic acid (18:4n3), EPA and DHA, make up around 30.8±6.6% of the total fatty acids.

As the daily mean I_{av} in the culture (Y_{avPBR}) increased over the course of the sets, the content of chlorophyll a (Chl a) in the biomass gradually decreased, ranging from a value of 1.145% d.w. at 42 $\mu E \cdot m^{-2} \cdot s^{-1}$ to 0.39% d.w. at 200 $\mu E \cdot m^{-2} \cdot s^{-1}$. Figure 2F shows the variation of the molar ratios of the main carotenoids of *C. rotallis*, normalised to Chl a. As expected, the molar ratio of fucoxanthin (*Fx*), a characteristic antenna pigment of *Chrysocromulina* (Rodríguez et al., 2006; Seoane et al., 2009), peaked at 0.992±0.010 at when the Y_{avPBR} value in the culture was 42 $\mu E \cdot m^{-2} \cdot s^{-1}$, ensuring photosynthesis even under conditions of low photon availability. Conversely, as Y_{avPBR} increased from 42 $\mu E \cdot m^{-2} \cdot s^{-1}$ to 200 $\mu E \cdot m^{-2} \cdot s^{-1}$, the

molar ratio of diatoxanthin (*Dtx*) gradually increased from 0.0188±0.0045 to 0.2188±0.0042, while the molar ratio of diadinoxanthin (*Ddx*) decreased from 0.3981±0.0186 to 0.2131±0.0119 (Figure 2F). This pattern represents a common photoprotective strategy of the photosynthetic system known as the diatoxanthin cycle (Pajot et al., 2023). The increase in *Dtx* is attributed to the de-epoxidation process of *Ddx* (*DES*) (Rodríguez et al., 2006; Seoane et al., 2009). Figure 2F demonstrates that with the increase in Y_{avPBR}, the *DES* value also rises, indicating a higher content of *Dtx* within the pool formed by *Ddx* and *Dtx*. These results are consistent with those reported for other strains of *Chrysocromulina* (Rodríguez et al., 2006; Seoane et al., 2009), and other haptophytes (Pajot et al., 2023) cultivated under varying irradiance levels. Thus, optimisation of available light intensity for cells is required to obtain the maximum fucoxanthin productivity. In this sense, the maximum fucoxanthin productivity was obtained in sets 1 and 2 (14.5±0.7 mg day^{-1}), while the maximum diatoxanthin productivity was achieved in sets 3-5 (5.0±0.4 mg day^{-1}).

As available irradiance increased throughout the sets, the total fatty acid content in microalgae increased from 12% to 19% dry weight. On contrast, the proportion of PUFAs on the total fatty acids decreased from 39% to 23% at the expense of an increase in saturated and monounsaturated fatty acids. This inverse relationship aligns with the findings of a prior investigation conducted on the haptophyte *Isochrysis galbana* as well (Abreu et al., 2019). The percentage of PUFAs over dry weight did not change significantly, with a mean value for all sets of 4.4 % ±0.3 %, in line with other studies (Santin et al., 2021). However, a recent literature review found that the effect of light intensity on lipid content in microalgae remains conflicting (Morales et al., 2021). While some studies suggest that light intensity has little effect on lipid content and accumulation, others have found that lipid content actually increases with higher light intensities until an optimum irradiance is reached for maximum lipid accumulation. Therefore, the effect of irradiance on fatty acid content may vary depending on factors such as the specific species of microalgae and the growth conditions used.

Extracts from the biomass of *C. rotalis* harvested in set 4 have recently been reported to have antiproliferative activity, which is desirable for potential use in pharmaceuticals,

cosmetics, or food supplements (González-Cardoso et al., 2023). The presence of PUFAs and carotenoids such as fucoxanthin, known for their antitumor properties, contributed to the observed activity, without precluding that the antitumor activity may also be influenced by unidentified metabolites. In this respect, the hemolytic activity detected in some microalgae extracts has been correlated with the presence of bioactive secondary metabolites (Abreu et al., 2019). The results of our study, displayed in Figure 3, also showed that *C. rotalis* in all sets had hemolytic activity, expressed as ESP, that was markedly dependent on experimental conditions. Thus, ESP increased close to 400% from set 1 to sets 4 and 5. This substantial increase appears to be primarily due to the escalating irradiance levels ($(Y_{av})_{max}$ in Table 1), with the most pronounced increase occurring between sets 1 and 4. In contrast, it is unlikely that reduced nutrient availability contributed significantly to this increase, as nutrients remained in surplus from set 2 onwards. This surplus is evident in Fig. 2D, where nutrient levels were far from exhausted at the end of each set. Consequently, the production of metabolites potentially associated with hemolytic activity did not appear to be significantly affected by nutrient availability. This observation is consistent with previous findings in *Chrysochromulina polylepis*, where hemolytic activity was induced during the light phase of culture, followed by a significant decrease during the dark phase (John et al., 2010). In our experiments, the proportion of light time within each light cycle was systematically increased across sets (see Table 1). On the contrary, the extract from set 6 did not present any hemolytic activity, indicating that the hyposaline shock completely repressed the synthesis of the possible metabolites responsible for the activity.

Comparatively to other haptophytes, the hemolytic activity of *C. rotalis* (ESP = 0.2) was similar to that measured for *I. galbana* (ESP=0.1), a microalga used in aquaculture (Shah et al., 2018), but almost 10 times lower than that reported for the dinoflagellate *Amphidinium* (ESP=2.4). In contrast, no hemolytic activity was detected in *N gaditana*, a microalga used as a supplement in fish feed. Regarding the genus *Chrysochromulina*, very high hemolytic activities have been reported in *C. polylepis*, the only one in this genus responsible for producing hemolytic toxins (John et al., 2010). Although the nature of the metabolites responsible for

hemolytic activities is known for some microalgae, such as amphidinols in *Amphidinium* (Kobayashi and Kubota, 2010), for *C. rotalis* it is still unknown. However, the selection of *C. rotalis* as a feedstock in biorefinery studies is justified by its potential to produce valuable bioactives. Future studies should aim to enhance the productivities of biomass and metabolites thereof by optimising nutrient supply, irradiance and operation mode.

4. Conclusions

The successful cultivation of *Chrysochromulina rotalis* in an LED-based tubular photobioreactor driven by a centrifugal pump demonstrated its superior tolerance to moderate shear stress (1.6 Pa) compared to other microalgae. The study showed that *C. rotalis* thrived without trace elements of Ni, V, and Cr, and that urea was an unsuitable nitrogen source. $NaH_2PO_4 \cdot H_2O$ or sodium glycerophosphate proved to be viable phosphorus sources. The design of the photobioreactor ensured consistent and reliable biomass production from shear-sensitive microalgae, highlighting its practical importance for sustainable biomass production in scientific and industrial contexts. *C. rotalis* holds promise as a valuable bioactive feedstock for biorefinery studies.

E-supplementary data of this work can be found in online version of the paper.

Acknowledgements

This research was funded by the State Research Agency (grants PID2019-109476RB-C22, RTC-2017-6405-1) of the Spanish Ministry of Science, Innovation and Universities; General Secretariat of Universities, Research and Technology of Andalusian Government (grant: P18-RT-2477); and the European Regional Development Fund Program.

No conflicts of interest, informed consent, or human or animal rights are applicable to this study.

References

1. Abreu, A.C., Molina-Miras, A., Aguilera-Saéz, L.M., López-Rosales, L., Cerón-Garciá, M.D.C., Sánchez-Mirón, A., Olmo-Garciá, L., Carrasco-Pancorbo, A., Garciá-Camacho, F., Molina-Grima, E., Fernández, I., 2019. Production of Amphidinols and Other Bioproducts of Interest by the Marine Microalga *Amphidinium carterae* Unraveled by Nuclear Magnetic Resonance Metabolomics Approach Coupled to Multivariate Data Analysis. J. Agric. Food Chem. 67(34), 9667-9682.
2. Acién Fernández, F.G., García Camacho, F., Sánchez Pérez, J.A., Fernández Sevilla, J.M., Molina Grima, E., 1997. A model for light distribution and average solar irradiance inside outdoor tubular photobioreactors for the microalgal mass culture. Biotechnol. Bioeng. 55(5), 701-714.
3. Andersen, R.A. 2005. Algal Culturing Techinques.
4. Bashir, K.M.I., Lee, J.H., Petermann, M.J., Shah, A.A., Jeong, S.J., Kim, M.S., Park, N.G., Cho, M.G., 2018. Estimation of antibacterial properties of chlorophyta, rhodophyta and haptophyta microalgae species. Microbiol. Biotechnol. Lett. 46(3), 225-233.
5. Bigelow, N., Barker, J., Ryken, S., Patterson, J., Hardin, W., Barlow, S., Deodato, C., Cattolico, R.A., 2013. Chrysochromulina sp.: A proposed lipid standard for the algal biofuel industry and its application to diverse taxa for screening lipid content. Algal Res. 2(4), 385-393.
6. Borowitzka, M.A., 2018. Biology of microalgae, in, Microalgae in health and disease prevention. Elsevier, pp. 23-72.
7. Cerón-García, M.C., González-López, C.V., Camacho-Rodríguez, J., López-Rosales, L., García-Camacho, F., Molina-Grima, E., 2018. Maximizing carotenoid extraction from microalgae used as food additives and determined by liquid chromatography (HPLC). Food Chem. 257(November 2017), 316-324.
8. Chen, B., Wan, C., Mehmood, M.A., Chang, J.S., Bai, F., Zhao, X., 2017. Manipulating environmental stresses and stress tolerance of microalgae for enhanced production of lipids and value-added products–A review. Bioresour. Technol. 244, 1198-1206.
9. Chisti, Y., 2009. Shear sensitivity. Encyclopedia of industrial biotechnology: bioprocess, bioseparation, and cell technology, 1-40.

10. Contreras, A., Garćıa, F., Molinaa, E., Merchuk, J.C., 1999. Influence of sparger on energy dissipation, shear rate, and mass transfer to sea water in a concentric-tube airlift bioreactor. Enzyme Microb. Technol. 25(10), 820-830.
11. de Vera, C.R., Crespín, G.D., Daranas, A.H., Looga, S.M., Lillsunde, K.E., Tammela, P., Perälä, M., Hongisto, V., Virtanen, J., Rischer, H., Muller, C.D., Norte, M., Fernández, J.J., Souto, M.L., 2018. Marine Microalgae: Promising source for new bioactive compounds. Mar. Drugs 16(9), 1-12.
12. Gallardo-Rodríguez, J.J., López-Rosales, L., Sánchez-Mirón, A., García-Camacho, F., Molina-Grima, E., 2015. Rapid method for the assessment of cell lysis in microalgae cultures. J. Appl. Phycol. 28(1), 105-112.
13. Gallardo-Rodríguez, J.J., López-Rosales, L., Sánchez-Mirón, A., García-Camacho, F., Molina-Grima, E., Chalmers, J.J., 2016. New insights into shear-sensitivity in dinoflagellate microalgae. Bioresour. Technol. 200, 699-705.
14. Glemser, M., Heining, M., Schmidt, J., Becker, A., Garbe, D., Buchholz, R., Brück, T., 2016. Application of light-emitting diodes (LEDs) in cultivation of phototrophic microalgae: current state and perspectives. Appl. Microbiol. Biotechnol. 100(3), 1077-1088.
15. González-Cardoso, M., Cerón-García, M., Navarro-López, E., Molina-Miras, A., Sánchez-Mirón, A., Contreras-Gómez, A., García-Camacho, F.J.B.T., 2023. Alternatives to classic solvents for the isolation of bioactive compounds from *Chrysochromulina rotalis*. Bioresour. Technol. 379, 129057.
16. Hikita, H., Asai, S., Kikukawa, H., Zaike, T., Ohue, M., 1981. Heat transfer coefficient in bubble columns. Industrial & Engineering Chemistry Process Design and Development 20(3), 540-545.
17. Hovde, B.T., Deodato, C.R., Hunsperger, H.M., Ryken, S.A., Yost, W., Jha, R.K., Patterson, J., Monnat, R.J., Barlow, S.B., Starkenburg, S.R., Cattolico, R.A., 2015. Genome Sequence and Transcriptome Analyses of *Chrysochromulina tobin*: Metabolic Tools for Enhanced Algal Fitness in the Prominent Order Prymnesiales (Haptophyceae). PLoS Genet. 11(9), 1-31.

18. John, U., Beszteri, S., Gloeckner, G., Singh, R., Medlin, L., Cembella, A.D.J.E.J.o.P., 2010. Genomic characterisation of the ichthyotoxic prymnesiophyte *Chrysochromulina polylepis*, and the expression of polyketide synthase genes in synchronized cultures. 45(3), 215-229.
19. John, U., Tillmann, U., Medlin, L.K., 2002. A comparative approach to study inhibition of grazing and lipid composition of a toxic and non-toxic clone of *Chrysochromulina polylepis* (Prymnesiophyceae). Harmful Algae 1(1), 45-57.
20. Kobayashi, J., Kubota, T., 2010. Bioactive metabolites from marine dinoflagellates. Comprehensive natural products II chemistry and biology 2, 263-325.
21. Leong, Y.K., Chen, C.Y., Varjani, S., Chang, J.S., 2022. Producing fucoxanthin from algae – Recent advances in cultivation strategies and downstream processing. Bioresour. Technol. 344(PA), 126170-126170.
22. López-Rosales, L., García-Camacho, F., Sánchez-Mirón, A., Martín Beato, E., Chisti, Y., Molina Grima, E., 2016. Pilot-scale bubble column photobioreactor culture of a marine dinoflagellate microalga illuminated with light emission diodes. Bioresour. Technol. 216.
23. López-Rosales, L., Sánchez-Mirón, A., García-Camacho, F., Place, A.R., Chisti, Y., Molina-Grima, E., 2018. Pilot-scale outdoor photobioreactor culture of the marine dinoflagellate *Karlodinium veneficum*: Production of a karlotoxins-rich extract. Bioresour. Technol. 253, 94-104.
24. Mayers, J.J., Flynn, K.J., Shields, R.J., 2014. Influence of the N: P supply ratio on biomass productivity and time-resolved changes in elemental and bulk biochemical composition of *Nannochloropsis* sp. Bioresour. Technol. 169, 588-595.
25. Michels, M.H.A., van der Goot, A.J., Vermuë, M.H., Wijffels, R.H., 2016. Cultivation of shear stress sensitive and tolerant microalgal species in a tubular photobioreactor equipped with a centrifugal pump. J. Appl. Phycol. 28(1), 53-62.
26. Mirón, A.S., Camacho, F.G., Gómez, A.C., Grima, E.M., Chisti, Y., 2000. Bubble-column and airlift photobioreactors for algal culture. AICHE J. 46(9), 1872-1887.

27. Molina-Grima, E., García-Camacho, F., Acién-Fernández, F.G., Sánchez-Mirón, A., Plouviez, M., Shene, C., Chisti, Y., 2022. Pathogens and predators impacting commercial production of microalgae and cyanobacteria. Biotechnol. Adv. 55(November 2021), 107884-107884.

28. Molina-Miras, A., López-Rosales, L., Sánchez-Mirón, A., Cerón-García, M.C., Seoane-Parra, S., García-Camacho, F., Molina-Grima, E., 2018a. Long-term culture of the marine dinoflagellate microalga *Amphidinium carterae* in an indoor LED-lighted raceway photobioreactor: Production of carotenoids and fatty acids. Bioresour. Technol. 265, 257-267.

29. Molina-Miras, A., Morales-Amador, A., de Vera, C.R., López-Rosales, L., 2018b. A pilot-scale bioprocess to produce amphidinols from the marine microalga *Amphidinium carterae*: Isolation of a novel analogue. Algal Res. 31(February), 87-98.

30. Molina, E., Fernández, J., Acién, F.G., Chisti, Y., 2001. Tubular photobioreactor design for algal cultures. J. Biotechnol. 92(2), 113-131.

31. Morales, M., Aflalo, C., Bernard, O., 2021. Microalgal lipids: A review of lipids potential and quantification for 95 phytoplankton species. Biomass Bioenergy 150, 106108.

32. O'Neill, E., 2020. Mining natural product biosynthesis in eukaryotic algae. Mar. Drugs 18(2), 90.

33. Ooms, M.D., Dinh, C.T., Sargent, E.H., Sinton, D., 2016. Photon management for augmented photosynthesis. Nature Communications 7(1), 1-13.

34. Pajot, A., Lavaud, J., Carrier, G., Lacour, T., Marchal, L., Nicolau, E.J.A.R., 2023. Light-response in two clonal strains of the haptophyte *Tisochrysis lutea*: Evidence for different photoprotection strategies. 69, 102915.

35. Ranganathan, P., Pandey, A.K., Sirohi, R., Hoang, A.T., Kim, S.H., 2022. Recent advances in computational fluid dynamics (CFD) modelling of photobioreactors: Design and applications. Bioresour. Technol., 126920.

36. Rhodes, L., Burke, B., 1996. Morphology and growth characteristics of *Chrysochromulina* species (Haptophyceae= Prymnesiophyceae) isolated from New Zealand coastal waters. N. Z. J. Mar. Freshwat. Res. 30(1), 91-103.

37. Rodríguez, F., Chauton, M., Johnsen, G., Andresen, K., Olsen, L., Zapata, M.J.M.B., 2006. Photoacclimation in phytoplankton: implications for biomass estimates, pigment functionality and chemotaxonomy. 148, 963-971.

38. Sánchez Mirón, A., Cerón García, M.C., García Camacho, F., Molina Grima, E., Chisti, Y., 2004. Mixing in bubble column and airlift reactors. Chem. Eng. Res. Des. 82(10), 1367-1374.

39. Santin, A., Russo, M.T., Ferrante, M.I., Balzano, S., Orefice, I., Sardo, A.J.M., 2021. Highly valuable polyunsaturated fatty acids from microalgae: Strategies to improve their yields and their potential exploitation in aquaculture. Molecules 26(24), 7697.

40. Sarkar, S., Manna, M.S., Bhowmick, T.K., Gayen, K., 2020. Priority-based multiple products from microalgae: Review on techniques and strategies. Crit. Rev. Biotechnol. 40(5), 590-607.

41. Seoane, S., Zapata, M., Orive, E., 2009. Growth rates and pigment patterns of haptophytes isolated from estuarine waters. J. Sea Res. 62(4), 286-294.

42. Shah, M.R., Lutzu, G.A., Alam, A., Sarker, P., Kabir Chowdhury, M.A., Parsaeimehr, A., Liang, Y., Daroch, M., 2018. Microalgae in aquafeeds for a sustainable aquaculture industry. J. Appl. Phycol. 30(1), 197-213.

43. Sirohi, R., Pandey, A.K., Ranganathan, P., Singh, S., Udayan, A., Awasthi, M.K., Hoang, A.T., Chilakamarry, C.R., Kim, S.H., Sim, S.J., 2022. Design and applications of photobioreactors-A review. Bioresour. Technol., 126858.

44. Sobczuk, T.M., Camacho, F.G., Grima, E.M., Chisti, Y., 2006. Effects of agitation on the microalgae *Phaeodactylum tricornutum* and *Porphyridium cruentum*. Bioprocess Biosystems Eng. 28(4), 243-250.

45. Tosun, I., 2007. Evaluation of Transfer Coefficients: Engineering Correlations. Second Edition ed, in: Tosun, I. (Ed.), Modeling in Transport Phenomena. Elsevier B.V., pp. 59-115.

46. Van de Waal, D.B., Smith, V.H., Declerck, S.A., Stam, E., Elser, J.J., 2014. Stoichiometric regulation of phytoplankton toxins. Ecol. Lett. 17(6), 736-742.

47. Vermuë, M.H., Eppink, M.H.M., Wijffels, R.H., Van Den Berg, C., 2018. Multi-product microalgae biorefineries: from concept towards reality. Trends Biotechnol. 36(2), 216-227.

48. Wang, C., Lan, C.Q., 2018. Effects of shear stress on microalgae – A review. Biotechnol. Adv. 36(4), 986-1002.

49. Wehr, J.D., Brown, L.M., 1985. Selenium requirement of a bloom-forming planktonic alga from softwater and acidified lakes. Can. J. Fish. Aquat. Sci. 42(11), 1783-1788.

50. Zeriouh, O., Reinoso-Moreno, J.V., López-Rosales, L., Cerón-García, M.d.C., Sánchez-Mirón, A., García-Camacho, F., Molina-Grima, E., 2017. Biofouling in photobioreactors for marine microalgae. Crit. Rev. Biotechnol. 37(8), 1006-1023.

Figure captions

Figure 1. Tubular photobioreactor system (tPBR) (A) Detailed photograph showing the physical embodiment of the tPBR. The photograph captures the intricate details of the system, including the tubes, LED-based lighting, system support structure and other relevant components. (B) Supervisory control and data acquisition (SCADA) diagram showing the various parts and their interconnections within the tubular photobioreactor system. The diagram provides a visual representation of the control and monitoring infrastructure used to ensure efficient operation and optimisation of the system.

Figure 2. **(A, B)** Influence of the concentration of nutrients in the different culture media (f/2, f/2 urea, K, K-PO4, L1+2Se) on **(A)** maximum biomass concentration and **(B)** maximum biomass productivity. The points correspond to the mean values. Bars around points represent 95% confidence intervals based on Fisher's least significant difference (LSD) procedure. Overlapping bars indicate no significant difference; thus, different lowercase letters represent experiments with significant differences (p-value <0.05) with a 95.0% confidence level. Erlenmeyer flasks of 100 mL with a 50-mL filling volume were used as culture vessels. **(C, D)** Dynamic progression of *Chrysochromulina rotalis* sequential cultivation in the tubular photobioreactor. Fluctuations over time in **(C)** biomass concentration (C_b), the daily mean irradiance inside the whole culture computed at the end of

each set (Y_{av}) and the maximum Y_{av} value supplied to the culture medium; **(D)** the concentrations of dissolved nitrate ([NO_3^-]) and phosphate ([$PO4^{-3}$]) in the supernatant are shown. The vertical dotted lines act as boundaries, distinguishing the different experimental sets carried out following the strategy outlined in Table 1. Data points are averages, and vertical bars are standard deviations (SD) for duplicate samples. **(E)** Daily mean absorbed volumetric photon flux (Γ_{av}; Eq. (9)) versus maximum biomass productivity (P_{bmax}) for each set. The daily mean values of the maximum photon flux (Γ_{max}), which the culture can potentially absorb in each set, are represented by horizontal dashed lines denote. **(F)** Variation of the molar ratio variation with respect to the Chl*a* concentration of the main carotenoids of *C. rotallis* and the de-epoxidation of diadinoxanthin (*Ddx*) to diatoxanthin (*Dtx*) (referred as *DES=Dtx/(Dtx+Ddx)*) as a function of the daily mean I_{av} in the culture (Y_{avPBR}) estimated for each set with Eq. 7.

Figure 3. Hemolytic activity measured as equivalent saponin potency, EPS (pg saponin per µg of biomass methanolic extract), in response to the experimental conditions imposed on each experimental set (see Table 1). Measurements were made on the biomass harvested at the end of each set. The points correspond to the mean values. Bars around points represent standard deviation. Different lowercase letters represent experiments with significant differences (p-value <0.05) with a 95.0% confidence level.

Accepted manuscript. https://doi.org/10.1016/j.biortech.2023.129818

Table 1. Summary of the strategy followed in this study. Six sets were defined depending on the modified culture characteristics such as the culture mode, the maximum daily mean irradiance supplied to the culture medium $(Y_{av})_{max}$ (given by Eq. 13 at $\gamma \rightarrow 0$), light:darkness cycle (hours), illumination pattern (sinusoidal al model during the lighting period, *Sns*, or continuous constant irradiance, *Cont*). It also appears the nutrient concentrations of nitrates and phosphate (µM) and N/P ratio of the culture medium used. The intervals are specified in days for each set. All irradiances are given at $\mu mol \cdot m^{-2} \cdot s^{-1}$.

Set	Interval	Culture mode	$(Y_{av})_{max}$	L/D cycle (pattern)	$[NO_3^-]_o$	$[PO_4^{3-}]_o$	$(N:P)_o$
1	0-2	Batch	25	12:12 (*Sns*)	5292	60	88:1
	3-9		50				
	9-13		127				
2	13-18	Fed-batch	238	16:8 (*Sns*)	4031	251	16:1
	18-22				1800	110	
3	22-44	Semicontinuous	800	20:4 (*Sns*)	5786	361	16:1
4	44-59		960	24:0 (*Cont*)	5400	337	16:1
5	59-78						
6	78-80	Hyposaline shock			540	33.7	

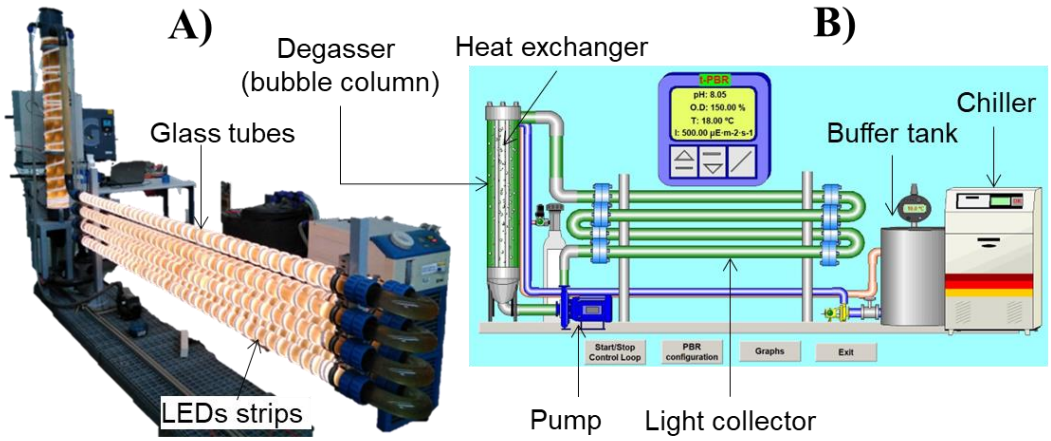

Figure 1

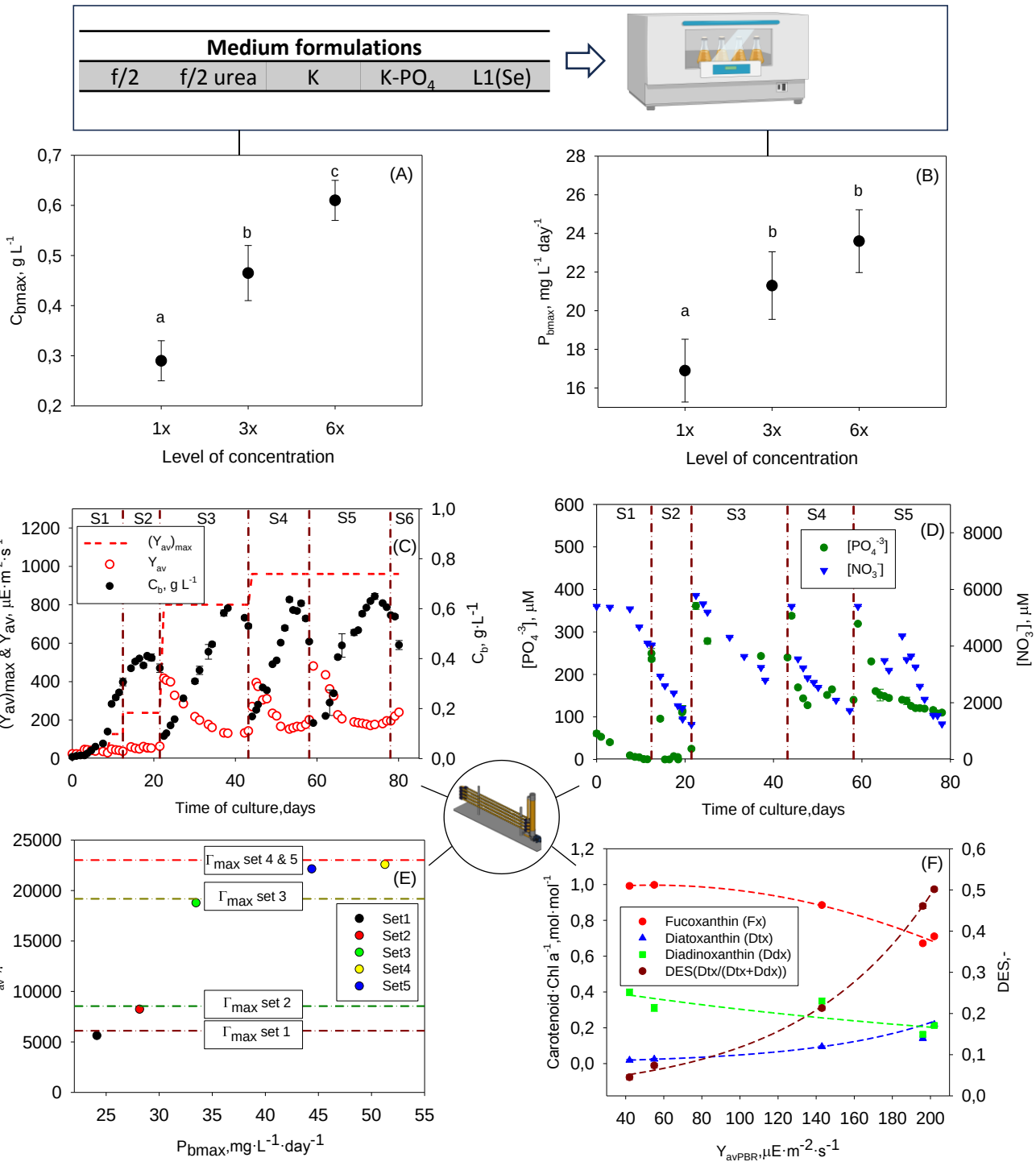

Figure 2

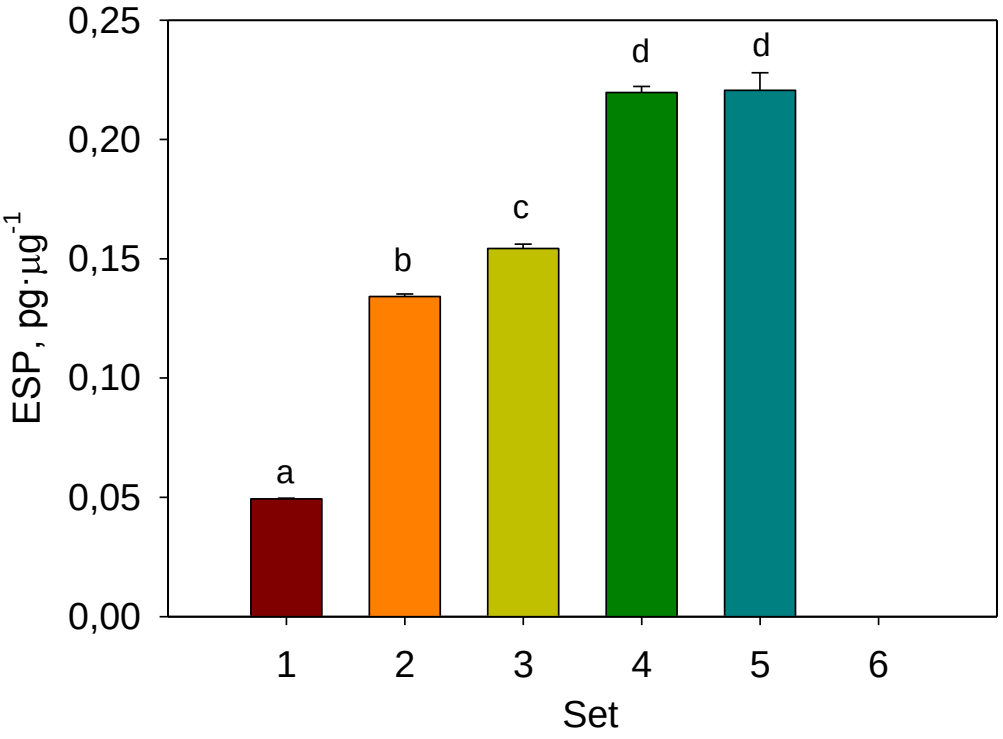

Figure 3

Accepted manuscript. https://doi.org/10.1016/j.biortech.2023.129818

CRediT author statement

Macías-de la Rosa, A.: Conceptualization, Data curation; Formal analysis; Investigation; Methodology; **López-Rosales, L.:** Conceptualization, Methodology, Formal analysis, Supervision, Writing - Original Draft, Project administration, Funding acquisition; **M.C. Cerón-García:** Conceptualization, Methodology, Formal analysis, Supervision, Writing - Original Draft, Project administration, Funding acquisition; **Molina-Miras, A.:** Investigation, Formal analysis, Validation, review; **Soriano-Jerez, Y.:** Investigation, Formal analysis, Validation, review; **Sánchez-Mirón, A.:** Conceptualization; Funding acquisition; Project administration; review & editing; **Seoane, S.:** Investigation, Formal analysis, Validation, review; **F. García-Camacho:** Conceptualization, Methodology, Formal analysis, Visualization, Supervision, Writing - Original Draft, Review & Editing, Project administration, Funding acquisition.